

# Accessible Color Cycles for Data Visualization

MATTHEW A. PETROFF, Johns Hopkins University, USA

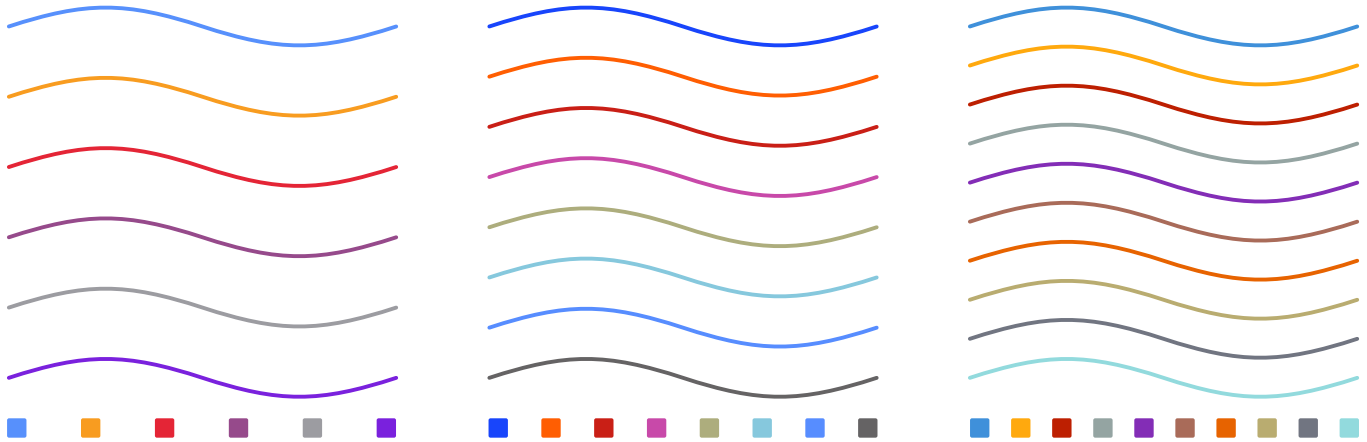


Fig. 1. Final color cycles derived in the present work. From left to right, the cycles containing six, eight, and ten colors are visualized as lines, ordered from top to bottom, and scatter plot points, ordered from left to right. The corresponding numeric color values are presented in Table 2.

Color cycles, ordered sets of colors for data visualization, that balance aesthetics with accessibility considerations are presented. In order to model aesthetic preference, data were collected with an online survey, and the results were used to train a machine-learning model. To ensure accessibility, this model was combined with minimum-perceptual-distance constraints, including for simulated color-vision deficiencies, as well as with minimum-lightness-distance constraints for grayscale printing, maximum-lightness constraints for maintaining contrast with a white background, and scores from a color-saliency model for ease of use of the colors in verbal and written descriptions. Optimal color cycles containing six, eight, and ten colors were generated using the data-driven aesthetic-preference model and accessibility constraints. Due to the balance of aesthetics and accessibility considerations, the resulting color cycles can serve as reasonable defaults in data-plotting codes.

CCS Concepts: • **Human-centered computing** → **Empirical studies in visualization**; *Accessibility design and evaluation methods*; • **Computing methodologies** → Discrete space search.

Additional Key Words and Phrases: color, scientific visualization, color-vision deficiency, crowdsourcing

## 1 INTRODUCTION

With the rise of electronic publishing starting in the 1990s, scientific visualization, in particular data plotting in scientific publications, switched from primarily using only black and white to primarily using color to represent variables and data. Although these new colorful plots are arguably more aesthetically pleasing, additional problems were introduced due to the somewhat arbitrary choice of colors. In the case of continuous variables, these shortcomings have been addressed with the introduction of perceptually-uniform colormaps such as *viridis* [van der Walt and Smith 2015] and *parula*

[Eddins 2014], which have begun to replace the use of severely-flawed rainbow colormaps such as *jet* [Moler 2015],<sup>1</sup> a subject on which much has been written [Crameri et al. 2020; Light and Bartlein 2004; Rogowitz and Treinish 1998]. The *cividis* colormap goes one step further, explicitly optimizing for both individuals with normal color vision and those with color-vision deficiencies [Nuñez et al. 2018].

Although there are no reliable global estimates, the prevalence of color-vision deficiencies is as high as 8% in certain sub-populations [Birch 2012]. Human color vision works through the use of long (L), medium (M), and short (S) wavelength color receptors, known as cones, which are sensitive to spectra perceived as red, green, and blue, respectively. Color-vision deficiencies, also commonly known as colorblindness, arise when one—or more—of these cones is either missing or has an altered spectral response. The most common types of color-vision deficiencies are deuteranomaly and protanomaly, which result from altered M and L cones, respectively. The complete lack of M or L cones, respectively known as deuteranopia and protanopia, is also somewhat common. Collectively, these four deficiencies are sometimes referred to as “red–green colorblindness,” since they affect the cones responsible for perceiving red or green, although red and green are not commonly confused with each other [Lillo et al. 2013]; instead, any color that contains the affected primary color is affected, e.g., protanopes have issues differentiating between blue and purple, since the red that is added to blue to form purple is not perceived. These common color-vision deficiencies are primarily hereditary. As they are caused by recessive genes linked to the X-chromosome, they primarily affect men [Neitz and Neitz 2011]. Altered S cone response and the lack of S cones are known as tritanomaly and tritanopia, respectively, but these conditions are

Author’s address: Matthew A. Petroff, Johns Hopkins University, Department of Physics & Astronomy, 3400 N Charles St, Baltimore, Maryland, 21218, USA, petroff@jhu.edu.

<sup>1</sup>Note that even improved rainbow colormaps such as *turbo* [Mikhailov 2019] are not accessible for individuals with color-vision deficiencies.

much less common, as is monochromacy, the complete lack of color vision [Sharpe et al. 1999].

While colormaps for plotting continuous variables have been improved in recent years based on research into perceptual uniformity, color cycles—ordered sets of colors used for categorical plotting,<sup>2</sup> e.g., line plots and scatter plots—have not received similar attention. Some alternatives have been proposed [Brewer et al. 2003; Okabe and Ito 2008], but they have been created based on a designer’s preferences instead of using data-driven derivations. Despite the prevalence of color-vision deficiencies, the default color cycles used in many plotting codes are not accessible to individuals without normal color vision. Accessible color cycles can be created through technical means by enforcing a minimum distance between colors in a perceptually-uniform color space and by using color-vision-deficiency simulations to also enforce the minimum distance for various color-vision deficiencies. However, a color cycle should also be aesthetically pleasing, to make it easier on the eyes and to encourage adoption of it, which is a matter of personal preference that cannot be directly accounted for with color-perception calculations. To address this, random accessible color cycles were generated and then presented as part of an online survey in an attempt to crowd-source data on aesthetic preference. The results of this survey were then used to train a machine-learning model to quantify aesthetic preference, which was in turn used to rank the randomly-generated color cycles in concert with accessibility constraints in order to select the ones that were both aesthetically pleasing and accessible, including to individuals with color-vision deficiencies.

The remainder of this paper is organized as follows. We start by discussing related work in Section 2, before moving on to cover a procedure for generating random accessible color sets in Section 3. Next, we discuss a color-cycle survey that was used to collect aesthetic-preference data in Section 4, a model constructed using the data in Section 5, and results from the model and other color-cycle-accessibility constraints in Section 6. Finally, we provide a discussion of the results in Section 7, before concluding in Section 8.

## 2 RELATED WORK

Previous work on color sets for visualization can primarily be categorized as designer color cycles, tools for creating custom color sets, and procedures for producing fixed color cycles that are optimal by a particular metric. There is also literature on adapting colors to a particular visualization, such as by using semantically-meaningful colors [Setlur and Stone 2016] or by accounting for feature adjacency or overlap [Lu et al. 2021], but such work will not be considered here further, since the goal of the present work is to devise generally-applicable color cycles. The most well-known work in the designer category is the *ColorBrewer* tool [Brewer et al. 2003], which presents a series of hand-crafted color cycles of various types, which were designed by an expert, primarily for use with visualizing data on a map. Also in this category is Okabe and Ito [2008], which presents a color cycle that was hand-crafted to maintain accessibility for color-vision-deficient individuals, and Zeileis et al. [2009], which presents a procedure for constructing color cycles.

<sup>2</sup>The phrase *color cycles* is used, since plotting codes will cyclically reuse colors in the cycle when the number of items to be plotted exceeds the number of colors in the cycle.

Two notable examples in the category of tools for creating custom color sets are the *I Want Hue* tool [Jacomy 2013], which uses a rule-based approach for guiding custom color set creation, and the *Colorgorical* tool [Gramazio et al. 2017], which combines a set of adjustable parameters with some degree of stochasticity to generate custom color sets that attempt to be both aesthetically-pleasing and accessible. Earlier rule-based tools, not specifically targeted at data visualization, include those described in Meier et al. [2004] and Hu et al. [2012]. Other tools not specifically targeted at data visualization are those of O’Donovan et al. [2011] and Mellado et al. [2017]. In O’Donovan et al. [2011], the authors developed an aesthetic-preference model based on color themes published in two different online communities for graphic designers to share such themes as well as survey data; they then used this model to develop tools for optimizing an input color cycle, for extracting a color cycle from an image, and for suggesting additional colors to extend a partial color cycle. In Mellado et al. [2017], a framework for interactive optimization of existing palettes is presented.

Finally, a significant example of optimizing to a metric is Glasbey et al. [2007], which alternatively used sequential search or simulated annealing to create color cycles that maximized the distance between colors in the CIELAB color space. Previously, Campadelli et al. [1999] had used a graph-based algorithm to find a color set that maximized the distance between colors in the CIELUV color space but with a more limited set of input colors. Earlier work with a similar goal—but published prior to the development of perceptually-uniform color spaces—is that of Kelly [1965]. Both Troiano et al. [2008] and Yanagida et al. [2014] presented algorithms for modifying existing color cycles to improve their accessibility to color-vision-deficient individuals.

Unfortunately, much of this previous work has generally not considered accessibility for color-vision-deficient individuals. Additionally, the existing data-driven approaches have generally not attempted to account for both aesthetic preference and accessibility.

## 3 GENERATING COLOR SETS

In order to create accessible color sets, a minimum perceptual distance between colors must be enforced. In this paper, the term *color set* is used to refer to a set of colors when their order does not matter, while the term *color cycle* is used when the order does matter. The perceptual distance between two colors is calculated by determining the Euclidean distance between the two colors,  $\Delta E'$ , in the CAM02-UCS perceptually-uniform color space [Luo and Li 2013]. This color space was designed such that a Euclidean distance of one between two color coordinates corresponds to an equal perceptual color difference throughout the color space for individuals with normal color vision. Note that observing conditions affect color perception, so the color-difference distance that corresponds to a just-noticeable difference depends on the observing conditions, including the size of the colored regions [Szafir 2018]. Regardless of the just-noticeable-difference color distance, larger distances correspond to easier-to-differentiate colors, which are more accessible.

In order to account for color-vision deficiencies, the method presented by Machado et al. [2009] is used to simulate the appearance

of colors for color-vision-deficient individuals,<sup>3</sup> and CAM02-UCS is then used to calculate and enforce a minimum perceptual distance for the transformed colors, with separate simulations performed for protanopia, deuteranopia, and tritanopia. The method presented in Machado et al. [2009] allows for simulating both dichromacy, the complete lack of one cone, and various severities of anomalous trichromacy, the shift in spectral response of a cone. The method was chosen due to this support of anomalous trichromacy, as well as since the method is physiologically-motivated and since the authors validated it to some degree with experimental data. Additionally, the same simulation and perceptual-distance calculation techniques were used in Nuñez et al. [2018] for creating the *cividis* colormap, except Nuñez et al. [2018] did not consider tritanopia. More specifically, we define the distance metric  $\Delta E_{\text{cvd}}$  for colors  $c_1$  and  $c_2$  as

$$\Delta E_{\text{cvd}}(c_1, c_2) = \min_{s \in \text{severities}} \min \left\{ \begin{array}{l} \Delta E'[c_1, c_2] \\ \Delta E'[\text{deut}_s(c_1), \text{deut}_s(c_2)] \\ \Delta E'[\text{prot}_s(c_1), \text{prot}_s(c_2)] \\ \Delta E'[\text{trit}_s(c_1), \text{trit}_s(c_2)] \end{array} \right\}, \quad (1)$$

where  $\Delta E'$  is the CAM02-UCS color distance and  $\text{deut}_s$ ,  $\text{prot}_s$ , and  $\text{trit}_s$  are the Machado et al. [2009] color-vision-deficiency simulation results for severity  $s$  for deuteranomaly, protanomaly, and tritanomaly, respectively. Unless otherwise noted, all integer severities are included,  $\{1 \dots 100\}$ . In addition, a minimum lightness distance,  $\Delta J'$ , is enforced to maintain accessibility for individuals with monochromacy and for accommodating grayscale printing. While calculations are performed using CAM02-UCS, colors are defined using 8-bit integer sRGB colors.

### 3.1 Creating a maximally-distant color cycle

As an alternative to allowing for aesthetic preference, a color cycle can instead be constructed in a manner that maximizes perceptual distance. Two such methods were proposed in Glasbey et al. [2007], one that used a sequential search algorithm starting with white as the first color and one that used simulated annealing, both operating in the CIELAB color space. CIELAB was an early attempt to create a perceptually-uniform color space [Fairchild 2013], which has been surpassed in accuracy by multiple more-recent color spaces including CAM02-UCS [Luo and Li 2013]. However, neither method took into account color-vision deficiencies, although the possibility of extending the methods to do so was discussed.

Here, we extend the sequential-search-algorithm method to use the perceptual-distance metric mentioned above,  $\Delta E_{\text{cvd}}$ . Additionally, we optionally allow the lightness range used to be restricted, although white is still included as the first color, regardless of the maximum allowed lightness. Two color cycles were generated using this method, one without lightness restrictions and one with a lightness restriction of  $J' \in [40, 90]$ , where  $J'$  is the CAM02-UCS lightness parameter. The lightness restriction is used because very dark and very light colors are generally poor choices for data visualization [Tufte 1990]. These cycles are shown in Table 1, along with

<sup>3</sup>The method presented in Machado et al. [2009] does not specify how its simulation matrices should be applied to RGB colors. This was noted by Harding et al. [2020], which also notes that the figures in Machado et al. [2009] were created by applying the simulation matrices to gamma-encoded sRGB values. Here, we apply the matrices to linear sRGB values, as was also done by Nuñez et al. [2018] and Harding et al. [2020].

Table 1. Maximally-distant color cycles constructed using the sequential method of Glasbey et al. [2007] extended to use CAM02-UCS and color-vision-deficiency simulations. The left half is the result when no lightness restriction is included, while the right half is the result when lightness is restricted to  $J' \in [40, 90]$ .

		$J' \in [0, 100]$				$J' \in [40, 90]$			
		R	G	B	$\Delta E_{\text{cvd}}$	R	G	B	$\Delta E_{\text{cvd}}$
■	0	0	0	100.0	■	0	69	254	67.8
■	41	101	255	59.4	■	156	58	0	61.8
■	163	99	0	54.0	■	144	142	158	37.5
■	72	72	84	33.1	■	255	161	0	36.1
■	1	247	0	32.8	■	108	75	125	24.2
■	156	155	173	32.2	■	170	205	255	23.5
■	0	0	165	28.8	■	89	144	255	22.6
■	94	32	0	26.7	■	255	24	90	21.3
■	222	187	164	21.0	■	211	186	175	20.6
■	85	124	103	20.6	■	37	255	130	15.4

the minimum perceptual distance between colors after each color is sequentially added to the cycle. These minimum distances will serve to inform the minimum distances used in the next section, where color sets will be generated with less-stringent constraints, to allow for optimization for aesthetic preference. Note that color sets with higher minimum perceptual distances than those in Table 1 can be found, since the simulated-annealing method of Glasbey et al. [2007] found a set of 11 colors with a minimum perceptual distance  $\sim 10\%$  higher than that of the cycle found by the corresponding sequential search algorithm.

### 3.2 Random set creation

In order to randomly generate accessible color sets, a Monte Carlo method is used. This process is agnostic to the exact minimum perceptual distance, and different constraints will be used when differently-sized color sets are desired, since a larger minimum perceptual distance can be enforced when fewer colors are needed. Since sRGB to CAM02-UCS conversions are computationally expensive, but the  $\sim 16.8$  million possible 8-bit sRGB colors easily fit in memory, the CAM02-UCS colors are precomputed for every possible color, both for normal color vision and for the three types of dichromacy. As with the previously-described sequential method, only colors with  $J' \in [40, 90]$  are used, where  $J'$  is the CAM02-UCS lightness value, leaving  $\sim 13.1$  million colors in the truncated gamut.

To generate a color set, a starting color is chosen at random. Then, each possible color is checked to see if it is far enough away in both lightness and perceptual distance, both for normal color vision and for color-vision deficiencies, at the maximum color-vision deficiency severity, dichromacy, i.e.,  $\Delta E_{\text{cvd}}$  is calculated for only a single severity, 100. Of these remaining colors, one is chosen at random using rejection sampling in the CAM02-UCS color space.<sup>4</sup> The process is then repeated until the color set contains the desired

<sup>4</sup>Due to a bug in the original version of the color-set-generation code that caused out-of-gamut colors to be wrapped into the sRGB gamut, the rejection sampling done for the initial sets was not done strictly in CAM02-UCS. This bug was identified and fixed before the final sets, described in Section 6.2, were generated.

number of colors or no colors matching the distance criteria remain in the sRGB gamut. Checking each possible color prior to rejection sampling is done as this method is guaranteed to complete in finite time—unlike rejection sampling alone—since rejection sampling is not performed when there are no remaining candidate colors. After the color set is generated, it is checked at intermediate levels of color-vision-deficiency severity to ensure that the minimum-perceptual-distance requirement is met there as well, i.e.,  $\Delta E_{\text{cvd}}$  is calculated with severities  $\{1 \dots 100\}$ . If the distance requirement is not met, the color set is thrown out. Checking a coarse color-vision-deficiency interval during set generation was tried but removed, since the performance penalty outweighed the gains from having to try again fewer times.

With this method in place, it is now possible to randomly generate color sets of various sizes that meet various minimum-perceptual-distance and minimum-lightness-distance requirements. Color sets containing six, eight, and ten colors were generated using this method, 10k of each size, with minimum perceptual distances of 20, 18, and 16, respectively; a minimum lightness distance of 2 was used in all three cases. The minimum perceptual distances were chosen as a compromise between maximizing accessibility and allowing for an expanded range of different color sets in order to allow for more leeway for aesthetic preference. The maximum minimum-perceptual distances among the sets of color sets were 24.3, 20.2, and 18.0 for the configurations with six, eight, and ten colors, respectively.

#### 4 COLOR-CYCLE SURVEY

While one could take an ontological approach to modeling aesthetic preference by trying to define a set of rules that make a pleasing color cycle, as is done by *I Want Hue* [Jacomy 2013], such a method is error-prone and substantially biased toward the personal preferences of the drafter of the rules. Instead of using ontologies, an alternative approach that is gaining traction in many fields is to infer a pattern from a large dataset using machine-learning techniques. This is the approach pursued here.

To this end, an online color-cycle survey was created.<sup>5</sup> After presenting the user with an introduction, a color-vision-deficiency questionnaire, and directions and after obtaining consent for the data collection, the primary survey started. In it, the user was presented with two color sets and was asked to choose the one that was, in the user’s opinion, more aesthetically pleasing as a gestalt. Then, four orderings of the chosen set were displayed, and the user again made a selection to taste. This basic process was then repeated again and again, with sets of either six or eight colors; there was no fixed end point. When the survey was first deployed, sets with ten colors were also presented, although this option was removed after a short period of time to increase the number of responses for the other two set sizes. For the choice of color set, each set was presented ordered by hue angle, since this makes the two sets easier to compare than if they were randomly ordered (or ordered by RGB values). Only two sets were presented to make for an easier choice. Additionally, a line-plot or scatter-plot rendering was shown with each color set when screen space was available, i.e., not on mobile devices. The line

thicknesses and marker sizes were randomly varied. A screenshot of the survey page is shown in Figure 2.

For the choice of ordering, four orders were presented, since multiple orderings are easier to compare than multiple sets, since the colors are all the same. Asking the user to order the colors to taste, instead of presenting possible orderings, was considered, but it was decided that while such an approach yields more information per response, it takes much longer and requires more effort, so each user would likely respond many fewer times. Thus, the simpler approach of presenting four possible ordering was taken.

The survey operated for approximately two years, from December 2018 through December 2020. It was promoted in user communities, primarily that of Matplotlib / Python, and was also linked to from banners on the author’s personal website<sup>6</sup> and that of the Pannellum panorama viewer [Petroff 2019]. Participation was entirely voluntary, and no compensation was offered. The survey collected ~22k responses from ~2.2k user sessions. More specifically, there were 10 347 six-color, 10 371 eight-color, and 1705 ten-color responses recorded. For 5.5% of the user sessions, the respondent self-identified as having some form of color-vision deficiency. Based on partial IP addresses, the countries, in decreasing order, with the largest number of user sessions were the United States, Germany, the United Kingdom, and Japan;<sup>7</sup> these four countries accounted for just over half of the user sessions.

#### 5 MODELING AESTHETIC PREFERENCE

In order to create a quantified measure of aesthetic preference, models must be constructed such that they can rank sets of color sets or color cycles, and model parameters must be able to be inferred from the pairwise responses collected using the previously-discussed survey. Ideally, these models should take a single color set or color cycle as an input and produce a continuous numerical output score, since this results in a simplified ranking process when compared to a model that takes two inputs and produces a binary-preference output. Additionally, a single model that works for a range of different color set or cycle sizes would be preferred, since it could be generalized to additional sizes. This would make it necessary to have only two models, one for scoring color sets and one for scoring color cycles for a given color set. To this end, a model was designed using an artificial-neural-network technique. Artificial neural networks consist of a set of units connected with trainable weights and nonlinear transformations and, given a sufficient number of parameters, can be used to approximate arbitrary functions [Russell and Norvig 2010].

To meet the requirement that the model can be trained using pairwise data while still producing a continuous numerical output score, a conjoined network architecture [Bromley et al. 1993] was chosen. In such an architecture, the outputs of two identical copies of a network with shared weights are connected together for the training process, in this case with a subtraction operation. Each copy takes one input from the training pair, and the result of the subtraction operation joining the outputs of the two copies is used to train the model using a binary-cross-entropy loss function. This

<sup>5</sup>While active, the survey was accessible at: <https://colorcyclesurvey.mpetroff.net/>

<sup>6</sup><https://mpetroff.net/>

<sup>7</sup>The 2019-12-24 release of the MaxMind GeoLite2 Country geolocation database was used to map partial IP addresses to countries.

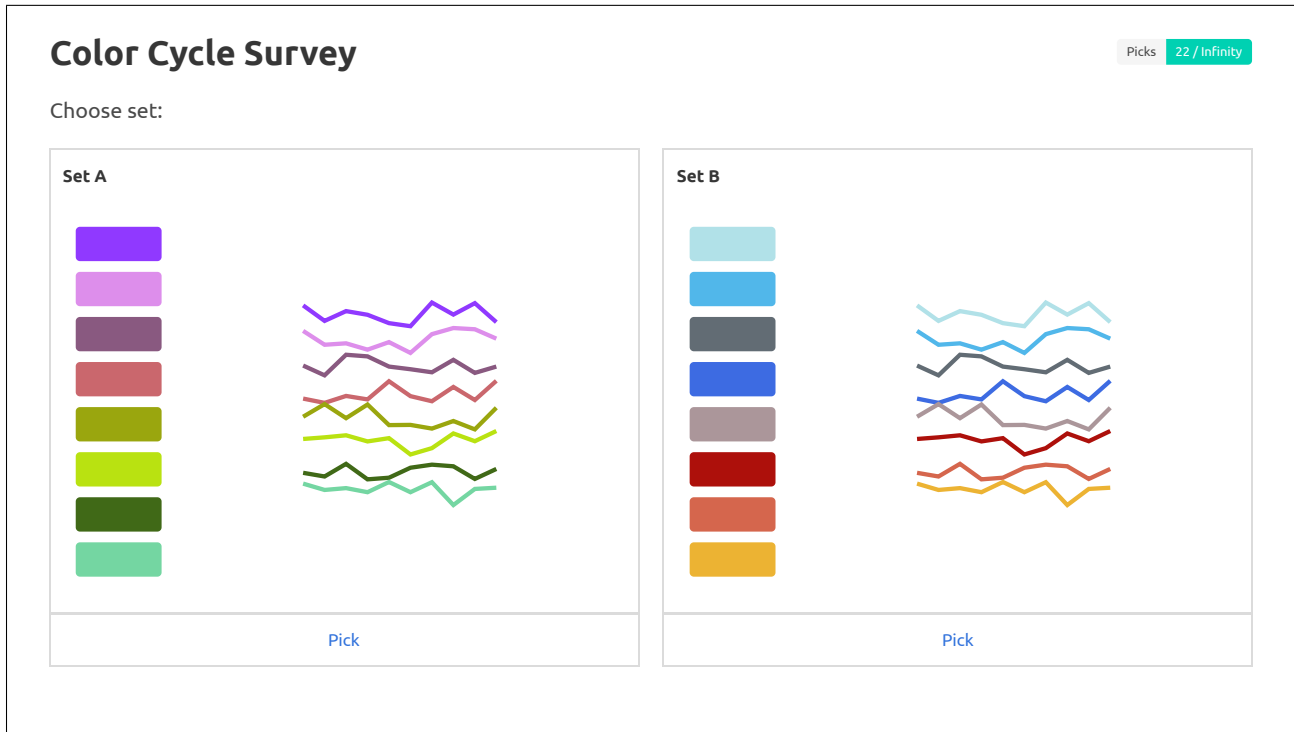


Fig. 2. Color survey sets interface. The survey respondent was presented with two separate color sets and asked to choose the more pleasing set; after this step, four possible orderings were presented, and the respondent was asked to choose the most pleasing ordering. The plot rendering was randomly changed between a line plot and a scatter plot, and different line thicknesses and marker sizes were used. The rendering was not shown on smaller screens and was not shown when picking orderings.

effectively trains each copy to produce a score for its input. Once the training process is complete, the joining operation is removed, and a single copy is used with a single input to produce an output score.

To allow a single model to be used with different input sizes, the model was designed to use a hybrid convolutional architecture. The individual colors in a color set or cycle are passed to the network as CAM02-UCS coordinates, divided by 100 for normalization. Each color is then passed through two dense, fully-connected network layers, each with five nodes. The weights for these layers are shared between each input color, so the number of input colors does not affect the number of weights in this portion of the network. These layers can be thought of as a way of learning an optimal encoding for the input colors. The outputs of the fully-connected layers are then passed through a set of three depthwise-separable convolution layers, with five, three, and one output channels, respectively; a kernel size of 5 is used, and the inputs are zero-padded before the kernel is applied such that the output shape is identical to the input shape. As these layers perform convolutions, they again do not depend on the number of input colors. Both the fully-connected layers and the convolution layers are each followed by an exponential linear unit (ELU) non-linear activation function [Clevert et al. 2016]. The output of the final convolution layer is averaged and then passed through a sigmoid activation function, producing an output score.

This is repeated for the second half of the conjoined network, and the two scores are differenced and passed through a final sigmoid activation function. A graphical overview of this architecture, which contains 167 trainable parameters, is presented in Figure 3.

The same model architecture is used for handling both the set data, where ordering does not matter, and the cycle data, where the ordering does matter. However, separate model instances are used. For the cycle data, there is one obvious choice for ordering the input data, the original cycle order, so this is what is used. The choice of ordering for the set data is not as straightforward. In the end, three orderings were used, corresponding to the set colors sorted along the three CAM02-UCS axes. A separate model instance was independently trained using each ordering on the same data, and the resulting output scores are averaged. This method was used as it was found to produce better results than using any of the axes individually or by ordering the colors based on hue angle.<sup>8</sup> The three-model ensemble has a total of 501 trainable parameters.

Ideally, the number of pairwise responses would greatly exceed the number of color sets with which to train the model. However, the number of responses is roughly equal to the number of color sets, and the response data have significant variance given that aesthetic preference is subjective and not always clear. Thus, care

<sup>8</sup>When the data were ordered by hue angle, the padding for the convolution layers was modified to cyclically wrap to avoid boundary effects.

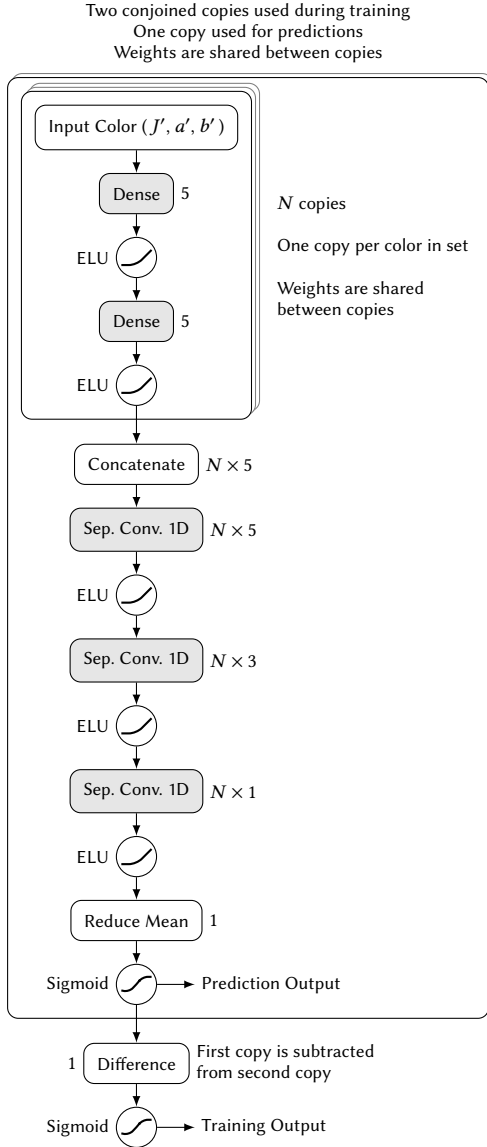


Fig. 3. Artificial-neural-network architecture overview. Shading denotes nodes with trainable parameters, and the numbers next to nodes denote their output dimensions. The 1D separable convolutions use a kernel of size 5, and the inputs are zero-padded before the kernel is applied such that the output shape is identical to the input shape. For the set model, the input colors were ordered along one of the three CAM02-UCS axes, and a separate copy of the model was independently trained for each ordering; the outputs of the three copies were then averaged. For the cycle model, the input colors were ordered per the cycle ordering.

must be taken to maximize the amount of information extracted from the survey data while preventing overfitting of the model and minimizing the effect of the data split and initialization values on the training process. To this end, bootstrap aggregation [Breiman 1996], i.e., bagging, was used to train a homogeneous ensemble of

100 models in parallel. For each model, training data were randomly drawn from the responses with replacement, creating 100 distinct training sets while still using all of the available data and allowing for overfitting to be checked for; each training set had a number of entries equal to 80% of the total number of survey responses for sets containing six colors. For each model, a test set was created using the responses not used in the training set. The outputs of the ensemble are averaged to produce the final output score. Data with six colors and with eight colors were used simultaneously during training but were treated separately when creating the training and test splits. Data with ten colors were not used.

The model ensembles were each trained, in a deterministic manner, for 120 epochs using the RMSprop optimization algorithm [Tieleman and Hinton 2012] with a learning rate of 0.01 and a batch size of 1024; L2 activity regularization was applied to all parameters with a value of 0.0001. Two separate model ensembles were trained, one for color sets and one for color cycles. In the case of color cycles, each response was converted from being a pick of the best of four possible orderings into three pairwise responses, i.e., the preferred ordering paired with each of the three worse orderings.

## 6 RESULTS

### 6.1 Performance of model

On the train set, the final set model achieved accuracies of 58.7% and 58.0% for the six-color and eight-color data, respectively. On the test set, it achieved accuracies of 57.8% and 57.0% for the six-color and eight-color data, respectively. The overall accuracies on the entire dataset were 58.2% and 57.5% for the six-color and eight-color data, respectively.<sup>9</sup>

The final cycle model achieved train-set accuracies of 54.4% and 54.6% for the six-color and eight-color data, respectively. On the test set, it achieved accuracies of 52.6% and 53.0% respectively. The overall accuracies on the entire dataset were 53.6% and 53.9% for the six-color and eight-color data, respectively.

As previously mentioned, sets with ten colors in them were presented as part of the color-cycle survey originally but were removed fairly early into the survey period, resulting in many fewer responses. As the training procedure required equal numbers of sets or cycles of different sizes, the ten-color data were excluded during training. However, this presented an opportunity for validating the model. After the model was finalized and its design, hyperparameter selection, and training were finished, the set and cycle models were evaluated on the ten-color data. With these data, the set model achieved an accuracy of 57.5%, identical to that achieved for the eight-color data. The cycle model achieved an accuracy of 52.2%.

As a cross-check on the machine-learning-derived color-set model, it was compared to a linear model based on summary statistics. The minimum, mean, and maximum of the chroma<sup>10</sup> and lightness values of each color set were used. Best-fit model parameters were inferred using a least-squares regression on the entirety of the survey data, where the differences between the summary statistics for the two sets in each response pair were regressed against the

<sup>9</sup>This is not quite the same as the weighted average of the train- and test-set accuracies due to the stochastic nature of bagging.

<sup>10</sup>Chroma is a measure of colorfulness and is related to—but not identical to—saturation.

binary preference value. This simple model had accuracies of 53.9%, 54.8%, and 54.6% for the six-color, eight-color, and ten-color sets, respectively, which are significantly less than the accuracies of the machine-learning model. Based on the linear model, the three most-significant summary statistics were, starting with the most significant, mean chroma, maximum chroma, and maximum lightness; higher mean chroma, lower maximum chroma, and lower maximum lightness values were the preferred trends for these summary statistics.

An additional comparison was made to the pair-preference model used as a proxy for color-set aesthetic preference in Gramazio et al. [2017] and based on data collected by Schloss and Palmer [2010]. This model scores color pairs using a linear-regression model based on coolness, hue similarity, and lightness contrast. To extend the pair-preference scores to a full color set, pair scores are calculated for each possible color pair in the set. In Gramazio et al. [2017], the color-set score was determined by using the minimum preference score of all the pairs. When applied to the color-set survey data collected in the present study, this method was found to offer little to no predictive power, with accuracies of 49.8%, 49.2%, and 50.1% for the six-color, eight-color, and ten-color sets, respectively. Calculating and using the mean of the pair-preference scores instead of the minimum, however, resulted in accuracies of 52.4%, 52.7%, and 54.4% for the six-color, eight-color, and ten-color sets, respectively.

## 6.2 Final color sets

Before using the trained aesthetic-preference model to select optimal color cycles, additional accessibility aspects need to be considered, specifically maximum lightness and compatibility with grayscale printing. Although the colors used in the survey were restricted in lightness with  $J' \leq 90$ , this is not necessarily enough for maintaining sufficient contrast with a white background for accessibility purposes. While no minimum-contrast standards exist for visualizations, such standards do exist for text, specifically the W3C Web Content Accessibility Guidelines 2.1 standard [Kirkpatrick et al. 2018], but these guidelines are not a good fit for visualizations.<sup>11</sup> As only two colors need to be considered for text content—the text color and the background color—much-stricter contrast guidelines can be used. Thus, following these guidelines, even those meant for large heading text, eliminates the use of most lighter colors. With fewer possibilities, the resulting color set must have a smaller minimum perceptual distance, which is problematic.

Fortunately, experimental data on how lightness affects plot readability has been collected, specifically by Smart and Szafrir [2019], who conducted an experiment where two scatter-plot markers of the same color and size but potentially of different shapes were presented along with gray distractor markers to research-survey respondents. The respondents were asked to answer as quickly and accurately as possible, and response times and accuracy were recorded, for markers of various CIELAB lightness,  $L^*$ .<sup>12</sup> In their analysis, the authors considered how lightness affects accuracy, finding that it decreased for  $L^* > 92$ . While only the use of extremely-light colors affected accuracy, darker—but still light—colors may also make it

difficult to discern marker shape and thus negatively affect the readability of a scatter plot. Smart and Szafrir [2019] published their raw data, allowing for a reanalysis of it in terms of how lightness affects response time; this reanalysis is described in Appendix A. It found that for 0.25°-size markers, response time increased for  $L^* > 84.6$ . As this value should be used as a minimum requirement and since color sets with fewer colors allow for more flexibility, stronger restrictions with increased readability can be placed on color sets with fewer colors. To this end, the minimum color distances for each set length are also used for minimum lightness distance from the white background, with lightness ranges of  $J' \in [40, 80]$ ,  $J' \in [40, 82]$ , and  $J' \in [40, 84]$  used for color sets of length six, eight, and ten, respectively.

Although the primary use-case for the color cycles being discussed here is use with emissive color-capable digital display devices, grayscale is a valid alternative display mode that still needs to be considered. Grayscale printing or display is handled by the lightness-difference restriction for monochromacy, although the original minimum difference,  $\Delta J' = 2$ , was deemed to be too small. It was increased to allow a maximum of three additional colors in the lightness range, resulting in a minimum  $\Delta J'$  of 5.0, 4.2, and 3.6 for sets of six, eight, and ten colors, respectively. Color printing was not specifically considered, since the printable gamut depends on the printing process and paper and thus results in much variability in appearance; however, the grayscale considerations also apply to color printing, so this omission is not a significant issue.

With these additional restrictions, new color sets were generated using the procedure described in Section 3.2. As these new color sets are drawn from a gamut that is a subset of the original gamut, the neural-network scoring model can be used without extrapolation. Again, 10k color sets were generated each for sets with six, eight, and ten colors. The maximum minimum-perceptual distances among these new sets of color sets were 23.6, 19.6, and 16.9 for the configurations with six, eight, and ten colors, respectively. These sets were each scored using the trained neural-network color-set model.

One last consideration to take into account is the interaction between color perception and language, since the easier a color is to name, the easier it is to refer to the color in a verbal or written description [Stone 2003]. Heer and Stone [2012] developed a probabilistic naming model for English based on several million crowdsourced color value–name pairs from the xkcd color survey [Munroe 2010]. In addition to naming given color values, this model can also produce color-saliency scores, which quantify the degree to which a color value can be uniquely named. A prototypical example of a commonly-used color name should have a high color-saliency score, while a color value that is on the transition between two commonly-used color names, e.g., halfway between pink and purple, should have a low color-saliency score. However, the existing model uses 153 color names, far more than the ~30 distinct names commonly used by untrained subjects [Derefeldt and Swartling 1995], and no attempt to merge color synonyms was made in its construction. As the existence of rarely-used color names or alternative color names does not affect the nameability of a color value in the same way that being on the transition between two commonly-used color names does, the large number of color names

<sup>11</sup>The guidelines also define color contrast in terms of the (linear) sRGB color space, which is not perceptually uniform.

<sup>12</sup>CIELAB lightness,  $L^*$ , is approximately equivalent to CAM02-UCS lightness,  $J'$ .

Rank	Six Colors	Eight Colors	Ten Colors
1			
2			
3			
4			
5			
6			
7			
8			
9			
10			
<hr/>			
9991			
9992			
9993			
9994			
9995			
9996			
9997			
9998			
9999			
10000			
<hr/>			
max(min $\Delta E_{cvd}$ )			

Fig. 4. Best and worst color sets. The ten highest-scored and ten lowest-scored color sets with six, eight, and ten colors, per the metric described in the text, are shown, starting with the set with the best score. Also shown is the color set, of the 10k randomly generated, with the maximum minimum-perceptual distance for each set length. Each color set is ordered by hue angle.

and lack of synonym merging negatively affects that usefulness of the existing model’s color-saliency metric. To remedy these shortcomings, the model was modified to merge color synonyms and remove rarely-used color names, a process that is described in Appendix B. The revised model was then used to score each of the previously-generated color sets, and the color-saliency scores were found not to correlate with the neural-network color-set scores. Final color-set scores were calculated by multiplicatively combining the neural-network color-set scores with the color-saliency scores, and the highest-scoring color sets with six, eight, and ten colors by this metric were selected as the final result. The ten highest-scored and ten lowest-scored color sets with six, eight, and ten colors by this metric are shown in Figure 4.

### 6.3 Final color cycles

All possible orderings of each of the highest-rated sets were then scored with the trained neural-network color-cycle model. This produced color cycles containing six, eight, and ten colors, which are each deemed to be near-optimal in an aesthetic sense by the neural-network models, given the accessibility restrictions used to generate them. However, there are additional aspects that should be considered to improve accessibility in the case when not all of the colors in the cycles are used. When only a subset of the colors are used, these colors should ideally be chosen to have a larger minimum

perceptual distance, including for color-vision deficiencies; have a larger minimum lightness distance, for grayscale display or printing; and be darker, to improve contrast with a white background. To this end, a cycle-accessibility metric is constructed as

$$\text{score}_{\text{accessibility}} = \frac{1}{N-1} \sum_{i=2}^N \min_{j \in [1, i)} \Delta E_{cvd}(i, j) \Delta J'(i, j), \quad (2)$$

where  $N$  is the number of colors in the cycle,  $\Delta E_{cvd}(i, j)$  is the perceptual distance—defined by Equation (1)—between the  $i^{\text{th}}$  and  $j^{\text{th}}$  colors of the cycle, and  $\Delta J'(i, j)$  is the lightness distance between the  $i^{\text{th}}$  and  $j^{\text{th}}$  colors of the cycle. This metric accounts for the perceptual-distance and lightness-distance considerations, preferring orderings where there are larger distances between colors earlier in the cycle. Before the metric is applied, white is added as the first color in the cycle, which causes orderings with darker colors toward the beginning of the cycle to be preferred.

An additional consideration comes from linguistic effects on color perception. The seminal work of Berlin and Kay [1969] identified eleven basic color terms, single-word terms that unambiguously refer to part of the color gamut. Since these terms are unambiguous, the use of color values that are all described by unique basic color terms makes it easier to refer to such values in written or verbal descriptions, when compared to color values that are described by the same color term. Additionally, previous research has shown that categorically-distinct colors can be discriminated between more rapidly than colors in the same category, even if the color pairs have the same perceptual distance [Winawer et al. 2007; Witzel and Gegenfurtner 2015]. To account for these effects, the probabilistic naming model described in Appendix B is applied to the colors in the color sets, and each color is assigned its most-probable basic color term. This information is then used to eliminate all orderings where a basic color term is repeated prior to all unique basic color terms in the color set being used.

Finally, the cycle machine-learning scores and cycle accessibility scores need to be combined. Since the first color in the cycle is the most important for aesthetic reasons, only the remaining orderings that start with the same color as that of the highest-ranked cycle per the machine-learning model are considered. After this data cut and the previous data cut with regard to repeated basic color terms, there are 48, 288, and 23 040 orderings remaining for the highest-scoring six-color, eight-color, and ten-color sets, respectively. The machine-learning scores and accessibility scores are then combined multiplicatively, and the highest-scoring color cycles with six, eight, and ten colors by this metric were selected as the final results, which are shown in Table 2 and Figure 1.

## 7 DISCUSSION

For the final results, all three color cycles start with blue, which is not surprising given that many existing color cycles start with blue and since blue is often a preferred color [Palmer and Schloss 2010]. Similarly, it is not surprising that the linear model, which was used as a cross-check, found that higher mean chroma but lower maximum chroma was preferred; existing advice suggests that more-saturated colors are preferable to a point [Palmer and Schloss 2010], but this should not be overdone to the point that the colors become

Table 2. Final color cycles for six, eight, and ten colors. The cycles are ordered from top to bottom, and sRGB values [0, 255] are given. The names shown are the most-probable names based on the color-naming model described in Appendix B. The minimum perceptual distances,  $\min \Delta E_{\text{cvd}}$ , take into account color-vision-deficiency simulations.

Six Colors					Eight Colors					Ten Colors				
	R	G	B	$\min \Delta E_{\text{cvd}}$		R	G	B	$\min \Delta E_{\text{cvd}}$		R	G	B	$\min \Delta E_{\text{cvd}}$
blue	87	144	252	100.0	blue	24	69	251	100.0	blue	63	144	218	100.0
orange	248	156	32	57.1	orange	255	94	2	66.9	orange	255	169	14	56.8
red	228	37	54	21.3	red	201	31	22	18.2	red	189	31	1	33.4
purple	150	74	139	21.3	purple	200	73	169	18.1	gray	148	164	162	22.3
gray	156	156	161	21.3	gray	173	173	125	18.1	purple	131	45	182	18.3
purple	122	33	221	20.5	light blue	134	200	221	18.1	brown	169	107	89	16.4
					blue	87	141	255	18.1	orange	231	99	0	16.3
					gray	101	99	100	18.1	tan	185	172	112	16.1
										gray	113	117	129	16.1
										light blue	146	218	221	16.1

gaudy [Tuft 1990]. Finally, the lack of correlation between the aesthetic-preference and color-saliency scores is consistent with the findings of Gramazio et al. [2017].

The various aesthetic and accessibility constraints considered in the above analysis are in some cases competing, so a balance had to be found. For example, maximizing lightness difference for grayscale display directly competes with the limiting of the lightness bounds, which was done both to avoid overemphasizing certain plotted features and to maximize contrast with a white background. The restrictions are also use-case dependent; while very-light colors are not acceptable for line plots or scatter plots, they could be fine when used to indicate areas on a map, particularly if boundaries are drawn in another color. As the goal was to make the resulting color cycles as generally-applicable as possible, the more conservative limits were chosen.

However, other considerations do not compete, so they can be more easily combined. The lack of correlation between aesthetic preference and color saliency is an example of this. While higher color saliency is not a factor in aesthetic preference, it does make it easier to name the colors in the cycle, which, in turn, makes it easier to describe them in written or verbal communication. However, since color saliency is language dependent [Kim et al. 2019], the use of this metric biases the results toward the use of color in the English language. While this might make the results less general, the aesthetic-preference score is arguably already biased toward English, since the survey used to collect the data behind it was conducted in English. Furthermore, the lack of correlation found between aesthetic preference and color saliency suggests any effect along these lines is minor and thus not a significant concern.

Although various accessibility aspects are considered here, including for color-vision deficiencies, color should still never be used as the sole means of communicating information. On data plots, line and marker styles should be varied when feasible, to give an additional factor by which to differentiate separate categories. Furthermore, these additional factors should also be used in written and verbal references to these features, such as in figure captions. While color-vision-deficient individuals have particular difficulty

with assigning names to colors, a color-only description is equally useless to anyone viewing a data plot in grayscale. Providing a visual example to go with a written reference, similar to what is generally done in plot legends, is also helpful but still does not replace the need to use an additional factor to describe the referenced features.

## 8 CONCLUSIONS

In this work, color cycles that balance aesthetics and accessibility were developed using a data-driven approach. Using a survey, data on color-cycle aesthetic preference was collected via crowdsourcing, and these data were used to construct machine-learning aesthetic-preference models. Optimal color cycles were then constructed by combining these aesthetic-preference models with accessibility constraints that address color-vision deficiencies, grayscale printing, minimum contrast with the background, and color saliency. As these are competing constraints, there is no correct answer as to how they should be combined. However, this work aimed to find a balance between aesthetics and various accessibility considerations, such that the resulting color cycles can serve as reasonable defaults in plotting codes. The survey data collected, the machine-learning aesthetic-preference model, and the code used to conduct the analysis and produce the results have been made available [Petroff 2021].

## ACKNOWLEDGMENTS

The author thanks the thousands of individuals who responded to the color-cycle survey, without whom these results would not exist. This work was made possible thanks to the Colorspacious [Smith et al. 2018], Matplotlib [Hunter 2007], Numba [Lam et al. 2015], NumPy [Harris et al. 2020], Scikit-learn [Pedregosa et al. 2011], SciPy [Virtanen et al. 2020], and TensorFlow [Abadi et al. 2016] libraries.

## REFERENCES

Martin Abadi, Ashish Agarwal, Paul Barham, Eugene Brevdo, Zhifeng Chen, Craig Citro, Greg S. Corrado, Andy Davis, Jeffrey Dean, Matthieu Devin, Sanjay Ghemawat, Ian Goodfellow, Andrew Harp, Geoffrey Irving, Michael Isard, Yangqing Jia, Rafal Jozefowicz, Lukasz Kaiser, Manjunath Kudlur, Josh Levenberg, Dan Mane, Rajat Monga, Sherry Moore, Derek Murray, Chris Olah, Mike Schuster, Jonathon Shlens,

- Benoit Steiner, Ilya Sutskever, Kunal Talwar, Paul Tucker, Vincent Vanhoucke, Vijay Vasudevan, Fernanda Viegas, Oriol Vinyals, Pete Warden, Martin Wattenberg, Martin Wicke, Yuan Yu, and Xiaoqiang Zheng. 2016. TensorFlow: Large-Scale Machine Learning on Heterogeneous Distributed Systems. *arXiv e-prints* (Mar 2016). arXiv:1603.04467 [cs.DC]
- Brent Berlin and Paul Kay. 1969. *Basic Color Terms: Their Universality and Evolution*. University of California Press, Berkeley / Los Angeles.
- Jennifer Birch. 2012. Worldwide prevalence of red-green color deficiency. *Journal of the Optical Society of America A* 29, 3 (Feb. 2012), 313–320. <https://doi.org/10.1364/josaa.29.000313>
- Leo Breiman. 1996. Bagging predictors. *Machine Learning* 24, 2 (Aug. 1996), 123–140. <https://doi.org/10.1007/bf00058655>
- Cynthia A. Brewer, Geoffrey W. Hatchard, and Mark A. Harrower. 2003. ColorBrewer in Print: A Catalog of Color Schemes for Maps. *Cartography and Geographic Information Science* 30, 1 (Jan. 2003), 5–32. <https://doi.org/10.1559/152304003100010929>
- Jane Bromley, Isabelle Guyon, Yann LeCun, Eduard Säckinger, and Roopak Shah. 1993. Signature Verification Using a ‘Siamese’ Time Delay Neural Network. In *Proceedings of the 6th International Conference on Neural Information Processing Systems* (Denver, Colorado) (NIPS ’93). Morgan Kaufmann Publishers Inc., San Francisco, California, 737–744.
- Paola Campadelli, Roberto Posenato, and Raimondo Schettini. 1999. An algorithm for the selection of high-contrast color sets. *Color Research & Application* 24, 2 (April 1999), 132–138. [https://doi.org/10.1002/\(sici\)1520-6378\(199904\)24:2<132::aid-col8>3.0.co;2-b](https://doi.org/10.1002/(sici)1520-6378(199904)24:2<132::aid-col8>3.0.co;2-b)
- Djork-Arné Clevert, Thomas Unterthiner, and Sepp Hochreiter. 2016. Fast and Accurate Deep Network Learning by Exponential Linear Units (ELUs). In *Proceedings of the 4th International Conference on Learning Representations* (San Juan, Puerto Rico) (ICLR ’16), Yoshua Bengio and Yann LeCun (Eds.). arXiv:1511.07289 [cs.LG]
- Fabio Cramer, Grace E. Shephard, and Philip J. Heron. 2020. The misuse of colour in science communication. *Nature Communications* 11, 1 (Oct. 2020), 5444. <https://doi.org/10.1038/s41467-020-19160-7>
- Gunilla Derefeldt and Tiina Swarthling. 1995. Colour concept retrieval by free colour naming. Identification of up to 30 colours without training. *Displays* 16, 2 (Jan. 1995), 69–77. [https://doi.org/10.1016/0141-9382\(95\)91176-3](https://doi.org/10.1016/0141-9382(95)91176-3)
- Steve Eddins. 2014. A New Colormap for MATLAB — Part 1 — Introduction. <https://blogs.mathworks.com/steve/2014/10/13/a-new-colormap-for-matlab-part-1-introduction/>
- Mark D. Fairchild. 2013. *Color Appearance Models* (3rd ed.). Wiley, Chichester, West Sussex.
- Chris Glasbey, Gerie van der Heijden, Vivian F. K. Toh, and Alison Gray. 2007. Colour displays for categorical images. *Color Research & Application* 32, 4 (2007), 304–309. <https://doi.org/10.1002/col.20327>
- Connor C. Gramazio, David H. Laidlaw, and Karen B. Schloss. 2017. Colorgical: Creating discriminable and preferable color palettes for information visualization. *IEEE Transactions on Visualization and Computer Graphics* 23, 1 (Jan. 2017), 521–530. <https://doi.org/10.1109/tvcg.2016.2598918>
- Lewis D. Griffin and Dimitris Mylonas. 2019. Categorical colour geometry. *PLOS ONE* 14, 5 (May 2019), e0216296. <https://doi.org/10.1371/journal.pone.0216296>
- Thomas H. Harding, Jon Vogl, Kharananda Sharma, and Juan Colon-Cruz. 2020. *An Analytical Evaluation of Unmanned Aircraft System Warning Signals as Processed by a Model of Color Deficiencies*. USAARL Report No. 2020-10. United States Army Aeromedical Research Laboratory. <https://apps.dtic.mil/sti/pdfs/AD1094561.pdf>
- Charles R. Harris, K. Jarrod Millman, Stéfan J. van der Walt, Ralf Gommers, Pauli Virtanen, David Cournapeau, Eric Wieser, Julian Taylor, Sebastian Berg, Nathaniel J. Smith, Robert Kern, Matti Picus, Stephan Hoyer, Marten H. van Kerkwijk, Matthew Brett, Allan Haldane, Jaime Fernández del Río, Mark Wiebe, Pearu Peterson, Pierre Gérard-Marchant, Kevin Sheppard, Tyler Reddy, Warren Weckesser, Hameer Abbasi, Christoph Gohlke, and Travis E. Oliphant. 2020. Array programming with NumPy. *Nature* 585, 7825 (Sept. 2020), 357–362. <https://doi.org/10.1038/s41586-020-2649-2> arXiv:2006.10256 [cs.MS]
- Jeffrey Heer and Maureen Stone. 2012. Color naming models for color selection, image editing and palette design. In *Proceedings of the SIGCHI Conference on Human Factors in Computing Systems* (Austin, Texas) (CHI ’12). ACM Press, New York, 1007–1016. <https://doi.org/10.1145/2207676.2208547>
- Guosheng Hu, Zhigeng Pan, Mingmin Zhang, De Chen, Wenzhen Yang, and Jian Chen. 2012. An interactive method for generating harmonious color schemes. *Color Research & Application* 39, 1 (Aug. 2012), 70–78. <https://doi.org/10.1002/col.21762>
- John D. Hunter. 2007. Matplotlib: A 2D Graphics Environment. *Computing in Science & Engineering* 9, 3 (2007), 90–95. <https://doi.org/10.1109/mcse.2007.55>
- Mathieu Jacomy. 2013. I Want Hue. <https://medialab.github.io/iwanthue/>
- Kenneth L. Kelly. 1965. Twenty-Two Colors of Maximum Contrast. *Color Engineering* 3, 6 (Dec. 1965), 26–27.
- Younghoon Kim, Kyle Thayer, Gabriela Silva Gorsky, and Jeffrey Heer. 2019. Color Names Across Languages: Salient Colors and Term Translation in Multilingual Color Naming Models. In *EuroVis 2019 - Short Papers* (Porto, Portugal), Jimmy Johansson, Filip Sadlo, and G. Elisabeta Marai (Eds.). The Eurographics Association, Geneva, Switzerland, 31–35. <https://doi.org/10.2312/evs.20191166>
- Andrew Kirkpatrick, Joshue O Connor, Alastair Campbell, and Michael Cooper. 2018. *Web Content Accessibility Guidelines (WCAG) 2.1*. W3C Recommendation. W3C. <https://www.w3.org/TR/2018/REC-WCAG21-20180605/>
- Siu Kwan Lam, Antoine Pitrou, and Stanley Seibert. 2015. Numba: a LLVM-based Python JIT compiler. In *Proceedings of the Second Workshop on the LLVM Compiler Infrastructure in HPC* (Austin, Texas) (LLVM ’15). ACM Press, New York, Article 7, 6 pages. <https://doi.org/10.1145/2833157.2833162>
- Lucien Le Cam and Grace Lo Yang. 2000. *Asymptotics in Statistics* (2nd ed.). Springer, New York. <https://doi.org/10.1007/978-1-4612-1166-2>
- Adam Light and Patrick J. Bartlein. 2004. The end of the rainbow? Color schemes for improved data graphics. *Eos, Transactions American Geophysical Union* 85, 40 (2004), 385–391. <https://doi.org/10.1029/2004eo400002>
- Julio Lillo, Humberto Moreira, Leticia Álvaro, and Ian Davies. 2013. Use of basic color terms by red-green dichromats: 1. General description. *Color Research & Application* 39, 4 (March 2013), 360–371. <https://doi.org/10.1002/col.21803>
- Kecheng Lu, Mi Feng, Xin Chen, Michael Sedlmair, Oliver Deussen, Dani Lischinski, Zhanglin Cheng, and Yunhai Wang. 2021. Palettaylor: Discriminable Colorization for Categorical Data. *IEEE Transactions on Visualization and Computer Graphics* 27, 2 (Feb. 2021), 475–484. <https://doi.org/10.1109/tvcg.2020.3030406> arXiv:2009.02969 [cs.GR]
- Ming Ronnier Luo and Changjun Li. 2013. CIECAM02 and Its Recent Developments. In *Advanced Color Image Processing and Analysis*, Christine Fernandez-Maloigne (Ed.). Springer, New York, 19–58. [https://doi.org/10.1007/978-1-4419-6190-7\\_2](https://doi.org/10.1007/978-1-4419-6190-7_2)
- Gustavo M. Machado, Manuel M. Oliveira, and Leandro A. F. Fernandes. 2009. A Physiologically-based Model for Simulation of Color Vision Deficiency. *IEEE Transactions on Visualization and Computer Graphics* 15, 6 (Nov. 2009), 1291–1298. <https://doi.org/10.1109/tvcg.2009.113>
- Barbara J. Meier, Anne Morgan Spalter, and David B. Karelitz. 2004. Interactive color palette tools. *IEEE Computer Graphics and Applications* 24, 3 (May 2004), 64–72. <https://doi.org/10.1109/mcg.2004.1297012>
- Nicolas Mellado, David Vanderhaeghe, Charlotte Hoarau, Sidonie Christophe, Mathieu Brédif, and Loïc Barthe. 2017. Constrained palette-space exploration. *ACM Transactions on Graphics* 36, 4 (July 2017), 1–14. <https://doi.org/10.1145/3072959.3073650>
- Anton Mikhailov. 2019. Turbo, An Improved Rainbow Colormap for Visualization. <https://ai.googleblog.com/2019/08/turbo-improved-rainbow-colormap-for.html>
- Cleve Moler. 2015. Origins of Colormaps. <https://blogs.mathworks.com/cleve/2015/02/02/origins-of-colormaps/>
- Randall Munroe. 2010. Color Survey Results. <https://blog.xkcd.com/2010/05/03/color-survey-results/>
- Jay Neitz and Maureen Neitz. 2011. The genetics of normal and defective color vision. *Vision Research* 51, 7 (April 2011), 633–651. <https://doi.org/10.1016/j.visres.2010.12.002>
- Jamie R. Nuñez, Christopher R. Anderton, and Ryan S. Renslow. 2018. Optimizing colormaps with consideration for color vision deficiency to enable accurate interpretation of scientific data. *PLOS ONE* 13, 7 (Aug. 2018), e0199239. <https://doi.org/10.1371/journal.pone.0199239> arXiv:1712.01662 [cs.CV]
- Peter O’Donovan, Aseem Agarwala, and Aaron Hertzmann. 2011. Color compatibility from large datasets. *ACM Transactions Graphics* 30, 4, Article 63 (July 2011), 12 pages. <https://doi.org/10.1145/1964921.1964958>
- Masataka Okabe and Kei Ito. 2008. Color Universal Design. <https://jfly.uni-koeln.de/color/>
- Stephen E. Palmer and Karen B. Schloss. 2010. An ecological valence theory of human color preference. *Proceedings of the National Academy of Sciences* 107, 19 (April 2010), 8877–8882. <https://doi.org/10.1073/pnas.0906172107>
- Fabian Pedregosa, Gaël Varoquaux, Alexandre Gramfort, Vincent Michel, Bertrand Thirion, Olivier Grisel, Mathieu Blondel, Peter Prettenhofer, Ron Weiss, Vincent Dubourg, Jake Vanderplas, Alexandre Passos, David Cournapeau, Matthieu Brucher, Matthieu Perrot, and Édouard Duchesne. 2011. Scikit-learn: Machine Learning in Python. *Journal of Machine Learning Research* 12 (2011), 2825–2830. <https://jmlr.org/papers/v12/pedregosa11a.html>
- Matthew A. Petroff. 2019. Pannellum: a lightweight web-based panorama viewer. *Journal of Open Source Software* 4, 40 (Aug. 2019), 1628. <https://doi.org/10.21105/joss.01628>
- Matthew A. Petroff. 2021. Creating accessible color cycles for data visualization. <https://github.com/mpetroff/accessible-color-cycles>
- Bernice E. Rogowitz and Lloyd A. Treinish. 1998. Data visualization: the end of the rainbow. *IEEE Spectrum* 35, 12 (Dec. 1998), 52–59. <https://doi.org/10.1109/6.736450>
- Stuart J. Russell and Peter Norvig. 2010. *Artificial Intelligence: A Modern Approach* (3rd ed.). Prentice Hall, Upper Saddle River.
- Karen B. Schloss and Stephen E. Palmer. 2010. Aesthetic response to color combinations: preference, harmony, and similarity. *Attention, Perception, & Psychophysics* 73, 2 (Nov. 2010), 551–571. <https://doi.org/10.3758/s13414-010-0027-0>
- Vidya Setlur and Maureen C. Stone. 2016. A Linguistic Approach to Categorical Color Assignment for Data Visualization. *IEEE Transactions on Visualization and Computer Graphics* 22, 1 (Jan. 2016), 698–707. <https://doi.org/10.1109/tvcg.2015.2467471>

- Lindsay T. Sharpe, Andrew Stockman, Herbert Jägle, and Jeremy Nathans. 1999. Opsin genes, cone photopigments, color vision, and color blindness. In *Color Vision: From Genes to Perception*, Karl R. Gegenfurtner and Lindsay T. Sharpe (Eds.). Cambridge University Press, Cambridge, Chapter 1, 3–52.
- Stephen Smart and Danielle Albers Szafrir. 2019. Measuring the Separability of Shape, Size, and Color in Scatterplots. In *Proceedings of the 2019 CHI Conference on Human Factors in Computing Systems (CHI '19)*. ACM Press, New York, 14 pages. <https://doi.org/10.1145/3290605.3300899>
- Nathaniel J. Smith, Richard Futrell, and Stéfan van der Walt. 2018. *Colorspacious*. <https://doi.org/10.5281/zenodo.1214904>
- Maureen C. Stone. 2003. *A Field Guide to Digital Color*. A. K. Peters, Natick, Massachusetts. <https://doi.org/10.1201/b12887>
- Danielle Albers Szafrir. 2018. Modeling Color Difference for Visualization Design. *IEEE Transactions on Visualization and Computer Graphics* 24, 1 (Jan. 2018), 392–401. <https://doi.org/10.1109/tvcg.2017.2744359>
- Tijmen Tieleman and Geoffrey Hinton. 2012. Lecture 6e: rmsprop: Divide the gradient by a running average of its recent magnitude. Coursera: Neural Networks for Machine Learning. [https://www.cs.toronto.edu/~tijmen/csc321/slides/lecture\\_slides\\_lec6.pdf](https://www.cs.toronto.edu/~tijmen/csc321/slides/lecture_slides_lec6.pdf)
- Luigi Troiano, Cosimo Birtolo, and Maria Miranda. 2008. Adapting palettes to color vision deficiencies by genetic algorithm. In *Proceedings of the 10th Annual Conference on Genetic and Evolutionary Computation (Atlanta, Georgia) (GECCO '08)*. ACM Press, New York, 1065–1072. <https://doi.org/10.1145/1389095.1389291>
- Edward R. Tufte. 1990. *Envisioning Information*. Graphics Press, Cheshire, Connecticut.
- Stéfan van der Walt and Nathaniel Smith. 2015. Matplotlib colormaps. <https://github.com/colormap/>
- Pauli Virtanen, Ralf Gommers, Travis E. Oliphant, Matt Haberland, Tyler Reddy, David Cournapeau, Evgeni Burovski, Pearu Peterson, Warren Weckesser, Jonathan Bright, Stéfan J. van der Walt, Matthew Brett, Joshua Wilson, K. Jarrod Millman, Nikolay Mayorov, Andrew R. J. Nelson, Eric Jones, Robert Kern, Eric Larson, C. J. Carey, İlhan Polat, Yu Feng, Eric W. Moore, Jake VanderPlas, Denis Laxalde, Josef Perktold, Robert Cimrman, Ian Henriksen, E. A. Quintero, Charles R. Harris, Anne M. Archibald, Antônio H. Ribeiro, Fabian Pedregosa, and Paul van Mulbregt. 2020. SciPy 1.0: Fundamental algorithms for scientific computing in Python. *Nature Methods* 17, 3 (Feb. 2020), 261–272. <https://doi.org/10.1038/s41592-019-0686-2> arXiv:1907.10121 [cs.MS]
- Jonathan Winawer, Nathan Witthoft, Michael C. Frank, Lisa Wu, Alex R. Wade, and Lera Boroditsky. 2007. Russian blues reveal effects of language on color discrimination. *Proceedings of the National Academy of Sciences* 104, 19 (April 2007), 7780–7785. <https://doi.org/10.1073/pnas.0701644104>
- Christoph Witzel and Karl R. Gegenfurtner. 2015. Categorical facilitation with equally discriminable colors. *Journal of Vision* 15, 8 (June 2015), 22. <https://doi.org/10.1167/15.8.22>
- Takuto Yanagida, Katsunori Okajima, and Hidenori Mimura. 2014. Color scheme adjustment by fuzzy constraint satisfaction for color vision deficiencies. *Color Research & Application* 40, 5 (Sept. 2014), 446–464. <https://doi.org/10.1002/col.21913>
- Achim Zeileis, Kurt Hornik, and Paul Murrell. 2009. Escaping RGBland: Selecting colors for statistical graphics. *Computational Statistics & Data Analysis* 53, 9 (July 2009), 3259–3270. <https://doi.org/10.1016/j.csda.2008.11.033>

## A MARKER-LIGHTNESS ANALYSIS

Experiment two of Smart and Szafrir [2019] examined how different colors and marker sizes affect the ability to discern different marker shapes on a scatter plot. Scatter plots with  $L^* = 50$  gray markers as distractors were shown with two colored markers, which were either the same shape or different shapes. The experiment used a binary-forced-choice design where the research subject was asked whether or not the two colored markers were identical, with instructions to complete the task as quickly and accurately as possible. The authors' analysis considered how changing the marker size and color affected accuracy and concluded that there was no significant effect except for decreased accuracy for markers with  $L^* > 92$ .

Smart and Szafrir [2019] kindly published their raw data, allowing for reanalysis. Here, the response time is considered instead of the accuracy. Even if two markers can be accurately told apart, the response time should increase if doing so is difficult. Only responses with the smallest marker size used in the experiments,  $0.25^\circ$ , are considered to look at the worst-case scenario; only correct responses are used. Furthermore, responses with response times less than half a second or more than ten seconds are excluded. The results of this

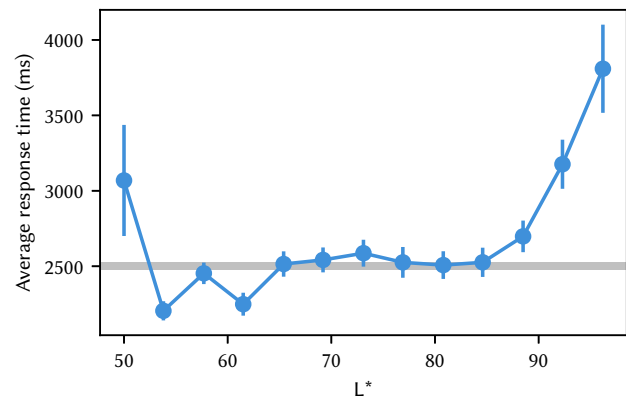


Fig. 5. Effect of scatter-plot marker lightness on response time. The average response time in milliseconds is shown for markers of various  $L^*$ , with error bars denoting the standard error. The horizontal gray band shows the overall mean, with a  $1\text{-}\sigma$  confidence interval. The data show that the use of colors with  $L^* > 84.6$  should be avoided to maintain scatter-plot readability.

analysis are shown in Figure 5. Response time significantly increased above the 2.5 s mean response time for  $L^* > 84.6$ , suggesting that only colors with lightness less than this threshold should be used in scatter plots to maintain readability. It also decreased somewhat for some of the darker markers, except for  $L^* = 50$ , which had increased response time. The fact that the distractors in the experiment were also of  $L^* = 50$  is a reasonable explanation for the increased response time for the  $L^* = 50$  markers.

## B COLOR-NAMING MODEL

Using several million crowdsourced color value–name pairs from the xkcd color survey [Munroe 2010], Heer and Stone [2012] developed a probabilistic naming model for English, which can be used to assign names to color values and to produce color-saliency scores. The saliency scores are meant to quantify the degree to which a color value can be uniquely named, which is a proxy for how easily a color value can be named. However, the construction of the model did not account for color synonyms, and the model uses far more color names than are commonly used. Since the existence of synonymous or rarely-used color names does not negatively affect the nameability of a color value to nearly the same degree that being partway between two commonly-used color names does, the model's lack of synonym merging and the inclusion of rarely-used color names degrades the usefulness of the model's saliency metric for determining how easily a color value can be named. Additionally, the lack of synonym merging can lead to sub-optimal color names for color values near the transition of two color names when multiple synonymous color names are used; for example, the model will use the term “blue” for lighter shades of blue than most people would, since while the combination of “light blue” and “sky blue” contains the majority of the probability for these color values, “blue” has a higher probability than either of the other two terms has individually.

The first step in improving the model is to identify and merge synonymous color names. Identifying the most-commonly-used color names as a function of color-gamut volume serves as a starting point for this process. The model discretizes the CIELAB color gamut into 8325 voxels and constructs a color-term count matrix,  $T$ , with a row for each voxel and a column for each color name. Thus, the set of most-commonly-used color names is constructed by calculating the most-probable color name for each voxel and using the color names that are the most-probable name for at least one voxel, resulting in a set of 33 names. Then, the distances between the probability distributions of each of these color names and the probability distributions of each of the other 152 color names in the model are calculated using the Hellinger distance [Le Cam and Yang 2000], defined as

$$D_h(w, v) = \sqrt{1 - \sum_c \sqrt{p(w|c)p(v|c)}}, \quad (3)$$

with a summation over all color values  $c$  in the discretized CIELAB color gamut and where  $w$  and  $v$  are color names and  $p(w|c)$  is the probability of color name  $w$  for color value  $c$ . Two color names are considered synonyms if the Hellinger distance between their probability distributions is less than 0.25, and the color names are merged by summing together the corresponding columns in the color-term count matrix. When synonyms were merged, the name most commonly provided by the survey respondents was used for the combined data.<sup>13</sup>

Next, rarely-used color names were eliminated from the model. To accomplish this, all color names that were not the most-probable name for at least one voxel or not merged with such a name were eliminated by dropping the corresponding columns from the model matrix. The revised model was then used to again find the most-probable color name for each voxel. The number of voxels where each of the eleven basic color terms identified by Berlin and Kay [1969] was the most-probable color name was tabulated, and “white” was found to be the term with the lowest voxel count; as noted in Heer and Stone [2012], this is likely because the xkcd color survey presented the color swatches to be named on a white background. Color names with a voxel count fewer than that of “white” were also eliminated by the previously-described method, leaving 28 color names in the final model. This number agrees well with previous estimates of 30 distinct color names used by untrained subjects [Derefeldt and Swartling 1995] and of the sRGB gamut containing 27 categorically-distinct regions of categorically-similar colors [Griffin and Mylonas 2019]. The color names in the final model, including synonyms, are shown in Table 3.

With the revised naming model, the color-saliency metric needs to be renormalized. As is done in Heer and Stone [2012], saliency is defined in terms of negative entropy ( $H$ ),

$$\text{saliency}(c) = -H(p(W|c)) = \sum_{w \in W} p(w|c) \log p(w|c), \quad (4)$$

where  $p(W|c)$  is the conditional probability of the name of a particular color value  $c$ , where  $p(w|c)$  is the probability of a given color name  $w$  for a given color value  $c$ , and where the summation is over

<sup>13</sup>This was not necessarily the same as the name that was the preferred name for the largest number of voxels.

Table 3. Color-naming-model names. The names in the left column are the 28 names remaining after the model of Heer and Stone [2012] was post-processed to merge synonyms and remove rarely-used names. The right column shows names that were determined to be synonymous to the corresponding names in the left column.

Name	Synonym(s)
green	
blue	
purple	violet
red	
pink	
yellow	
orange	
brown	
teal	turquoise, blue-green
light blue	sky blue
gray	
lime green	lime
magenta	fuchsia
light green	
cyan	aqua
dark blue	navy blue*
dark green	forest green
olive	
lavender	light purple, lilac
black	
tan	
yellow-green	green-yellow, chartreuse
maroon	burgundy
salmon	
peach	
beige	
mustard	gold, dark yellow, mustard yellow
white	

\* As part of the data pre-processing performed in Heer and Stone [2012], all instances of “navy” were converted to “navy blue,” so both terms should be considered synonyms.

all color names in the model. The saliency is calculated for all voxels in the revised model, giving a saliency range of approximately  $-3.158$  to  $0$ ; the minimum and maximum saliency values are then used to normalize the saliency metric to  $[0, 1]$ .

With the revised model, linear interpolation in the CIELAB color space, instead of binning, is used to calculate color names and saliencies. Colors are named by interpolating the probabilities of each color name separately and using the interpolated probabilities to determine the most-probable name. For saliencies, the voxel saliency values are directly interpolated.